American Mineralogist, Volume 79, pages 960–972, 1994

Forward modeling of calc-silicate microinclusions and fluid evolution in a graphitic metapelite, northeast Sardinia

J.A.D. Connolly
Institute for Mineralogy and Petrography, Swiss Federal Institute of Technology, Zurich CH-8092, Switzerland
I. Memmi
Dipartimento di Scienze della Terra, Università di Siena, via delle Cerchia 3, Siena I-53100, Italy
V. Trommsdorff
Institute for Mineralogy and Petrography, Swiss Federal Institute of Technology, Zurich CH-8092, Switzerland
M. Franceschelli
Dipartimento di Scienze della Terra, Università di Cagliari, via Trentino 51, Cagliari I-09127, Italy
C. A. Ricci
Dipartimento di Scienze della Terra, Università di Siena, via delle Cerchia 3, Siena I-53100, Italy

Abstract

The primary microinclusion assemblage anorthite ± margarite ± epidote occurs within garnet and rutile in a graphitic metapelite from northeast Sardinia. The existence of the microinclusion assemblage and the observed paragenetic sequence and mineral compositions for the entire rock are in good agreement with phase relations predicted from thermodynamic data for the system CaO-Na_2O-K_2O-MgO-FeO-Al_2O_3-SiO_2-TiO_2-C-O-H. The complexity of the microinclusion phase relations is reduced by the specification of a component saturation hierarchy that permits thermodynamic projection through phases of variable composition. The microinclusion assemblage is predicted to be stable over the pressure and temperature intervals of 6585–6685 bars and 550–575 °C, with a C-O-H fluid of composition $X_O = 0.46$–0.57 (ca. 26–45 mol% CO_2), where X_O represents the atomic fraction of total O relative to O + H in the fluid phase. The assemblage anorthite + potassium feldspar + albite + muscovite + quartz, present within other garnets, requires an even more CO_2-rich fluid composition with $X_O > 0.9$ (ca. 89 mol% CO_2). With progressive metamorphism, fluid composition was buffered toward more H_2O-rich fluid compositions by the minute calc-silicate domains represented by the microinclusions. The CO_2 fluid compositions represent a significant deviation from those generated by simple dehydration in the presence of graphite ($X_O = ⅓$) and suggest that an additional source of O was contributed to the fluid, most probably as CO_2. Because the buffering capacity of the calc-silicate domains would be overwhelmed by any significant fluid influx, an external source of CO_2 is improbable. No internal source of CO_2 is preserved, but the calcic character of the inclusions and the high-X_O fluid compositions could be explained by carbonate in the metapelite protolith. The calc-silicate inclusions record an interval of the metamorphism during which low rates of fluid production and infiltration inhibited bulk equilibration. This interval was terminated by an episode of dehydration that introduced more voluminous quantities of fluid into the rock. These results suggest that fluid from adjacent rocks had not permeated the metapelite when the inclusions formed and provide an argument against the importance of pervasive fluid movement during a stage of the prograde metamorphism.

Introduction

Thermobarometry and estimation of fluid composition from mineral equilibria are done almost invariably by an inverse approach in which it is assumed that observed mineral compositions represent stable equilibrium compositions. These mineral compositions are then used to make activity corrections to compute the displacement of equilibria in some chemical subsystem of the rock. Drawbacks of this method are that it provides no test for the equilibrium assumption and that the reactions corresponding to the equilibria in the chemical subsystem often bear little resemblance to actual metamorphic processes. An alternative approach to fixed composition methods is to compute equilibria for the full chemical

0003–004X/94/0910–0960$02.00

system, or a close approximation thereof, and compare predicted and observed mineral assemblages, i.e., forward modeling. This approach has the advantages that it provides a rigorous test for consistency between the observed mineral compositions and the thermodynamic models used to describe mineral behavior and that the computed reactions correspond to those observed in nature. The feasibility of this approach is often limited by the complexity of the computed phase relations (e.g., Powell and Holland, 1990). This paper demonstrates a method of reducing this complexity by specification of a component saturation hierarchy (Connolly, 1990) that permits phase diagram projection through the compositions of mineral solutions.

Forward modeling is applied here to determine the petrological significance of plagioclase (anorthite), margarite, and zoisite microinclusions within grossular-rich garnets in a graphitic metapelite from northeast Sardinia. In contrast to the plagioclase inclusions described by Whitney (1991), these inclusions show no evidence of modification subsequent to entrapment. The interpretation of the inclusion phase equilibria offers insights into the physicochemical conditions and nature of fluid-rock interaction during the metamorphism.

Geologic setting

The predominant rocks in the Hercynian basement of the Gallura region (Fig. 1) are metasedimentary, with metamorphic grade increasing from the chlorite zone in the south through biotite, garnet, staurolite + biotite, kyanite + biotite, and sillimanite + potassium feldspar zones northward (Franceschelli et al., 1982). The high-grade zones of this sequence formed during the last major episode of metamorphism in the region, which was coeval with a major deformation phase (Franceschelli et al., 1989). Within porphyroblasts there is textural evidence for several cycles of deformation. Earlier petrologic analysis of the matrix mineral assemblage and porphyroblasts from rocks in the Gallura region suggests peak metamorphic temperatures of about 620 °C during a period of decompression from 10 to 4 kbar (Franceschelli et al., 1989).

Sampling and analytic methods

In the course of a study of the metamorphic basement of the Gallura region, 15 metapelite samples were collected from a lens (1 × 0.2 km) of a graphitic mica schist within migmatites near the high-grade limit of the kyanite + biotite zone (Fig. 1). The major mineral content and texture are similar in all 15 samples, but the single sample discussed here is unique in that it contains calc-silicate microinclusions. The microinclusions were identified and analyzed, with the exception of rutile and ilmenite, by energy-dispersive X-ray analysis on a Phillips 515 scanning electron microscope at the University of Siena (see Franceschelli et al., 1989, for analytic details). Accuracy with this method is ±1 wt% for the major oxides. Rutile and ilmenite were analyzed by wavelength-dispersive analysis with a Cameca SX50 electron microprobe at the Swiss Federal Institute of Technology. The microprobe analyses were done with a 20-s counting time, 20-nA sample current, 15-kV acceleration voltage, and 2-μm beam width, using quartz, rutile, corundum, tephroite, periclase, and wollastonite as standards.

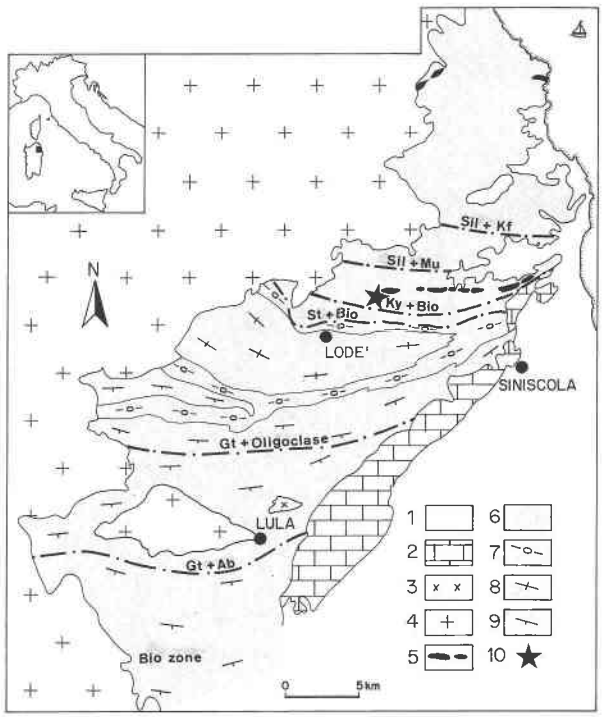

Fig. 1. Geologic map of the Gallura region (modified after Elter et al., 1986) with metamorphic isograds. Map symbols: (1) recent and plio-quaternary deposits; (2) mesozoic platform carbonate sediments, continental and lagoonal sediments, and evaporites; (3) acid porphyritic dikes; (4) Hercynian granitoids; (5) amphibolites and partially retrogressed eclogites; (6) migmatitic complex; (7) rhyolitic augen gneiss; (8) granodioritic orthogneiss; (9) mica schists and paragneisses; (10) sample locality.

Petrography

The metapelite consists of large (1–5 mm) porphyroblasts of staurolite, kyanite, and quartz, enveloped in a mixture of muscovite and biotite and included in a matrix of quartz, biotite, oligoclase, muscovite, and ilmenite (Fig. 2a). Garnet occurs as small rounded porphyroblasts and, more commonly, as euhedral inclusions (100–400 μm) in staurolite (Fig. 2a and 2c), in plagioclase (Fig. 2d), and rarely in kyanite porphyroblasts. With the exception of a few clear garnet inclusions in the cores of staurolite porphyroblasts, the garnet is cloudy from the presence of abundant fluid and solid inclusions (Figs. 2b, 2d, and 3a) and shows some evidence of reaction of plagioclase and biotite. The clear garnets contain minute primary fluid inclusions, the high refractive index of which suggests they are CO_2-rich. In contrast, the clouded garnets contain relatively abundant low refractive-index fluid inclu-

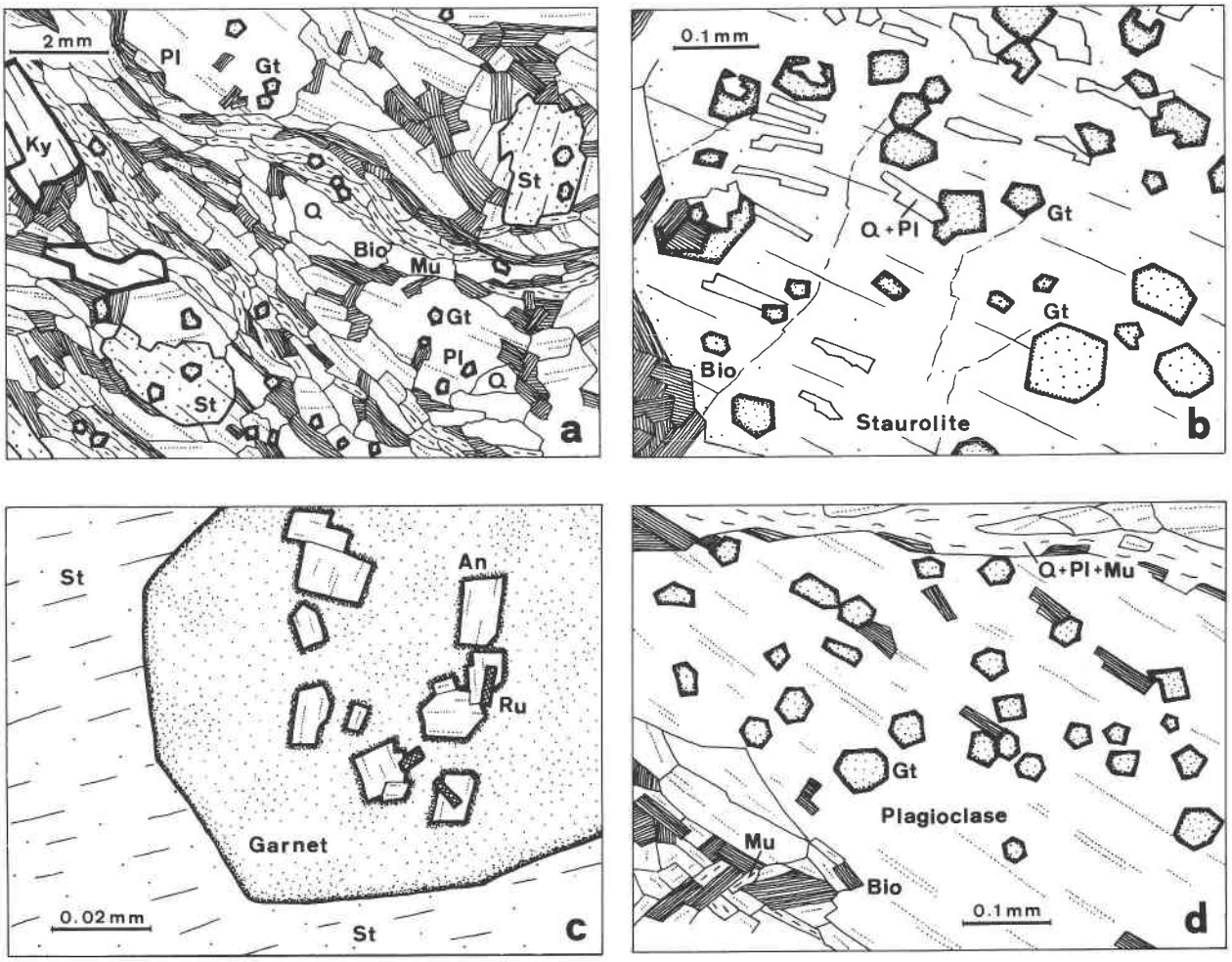

Fig. 2. Sketches from metapelite photomicrographs (see Table 1 for notation): (**a**) matrix; (**b**) clear (lower right) and cloudy garnet inclusions within staurolite; (**c**) anorthite within a clear garnet inclusion; (**d**) cloudy garnet inclusions within plagioclase.

sions that are probably H_2O-rich. Finely disseminated graphite is present throughout the rock.

The clear garnets contain calc-silicate microinclusions (<20 μm) of idiomorphic anorthite (or anorthite-rich plagioclase), epidote, and margarite (Fig. 3b). Typically muscovite, quartz, rutile, and ilmenite are also present as microcinclusions. In one case, anorthite, albite, and potassium feldspar were observed together with muscovite and quartz (Fig. 3c). The clouded garnets contain only plagioclase, muscovite, quartz, rutile, and ilmenite. In addition to the garnet inclusions, plagioclase and staurolite porphyroblasts contain rutile (100–200 μm), which is often partially rimmed by, and contains lamellae of, ilmenite. The rutile grains contain <10-μm grains of anorthite, epidote, margarite, muscovite, paragonite, and quartz (Fig. 3d). Rutile is also present within some matrix biotite. There is no textural evidence of disequilibrium in the calc-silicate microinclusions within the garnet and rutile, but in some cases paragonite and muscovite form intimate intergrowths, which may indicate exsolution during cooling. The paragenetic sequence for the observed metapelite mineral assemblage, as inferred from textural relationships, is summarized in Figure 4.

Mineral solution notation

The description of mineral solutions involving mixing on two or more independent sublattices (Hillert, 1980) is cumbersome because of the number of end-members involved. To simplify this, compositions are expressed here in terms of the magnitude of the compositional vectors necessary to obtain the composition of interest from the composition of one end-member (see Thompson, 1981). Specifically, the notations $Bio_{x,y,z}$, $Chl_{x,y}$, and $Mu_{x,y,z}$ symbolize the biotite, chlorite, and muscovite compositions:

$$Bio_{x,y,z} = KMg_{(3-y-3z)x}Fe_{(3-y-3z)(1-x)}Al_{1+2y+2z}Si_{3-y}O_{10}(OH)_2$$

$$= KFe_3AlSi_3O_{10}(OH)_2 \text{ (annite)} + xMgFe_{-1}$$

$$+ yAl_2M_{-1}Si_{-1} + zAl_2M_{-3}$$

$$Chl_{x,y} = Mg_{(5-y)x}Fe_{(5-y)(1-x)}Al_{4+2y}Si_{3-y}O_{10}(OH)_8$$

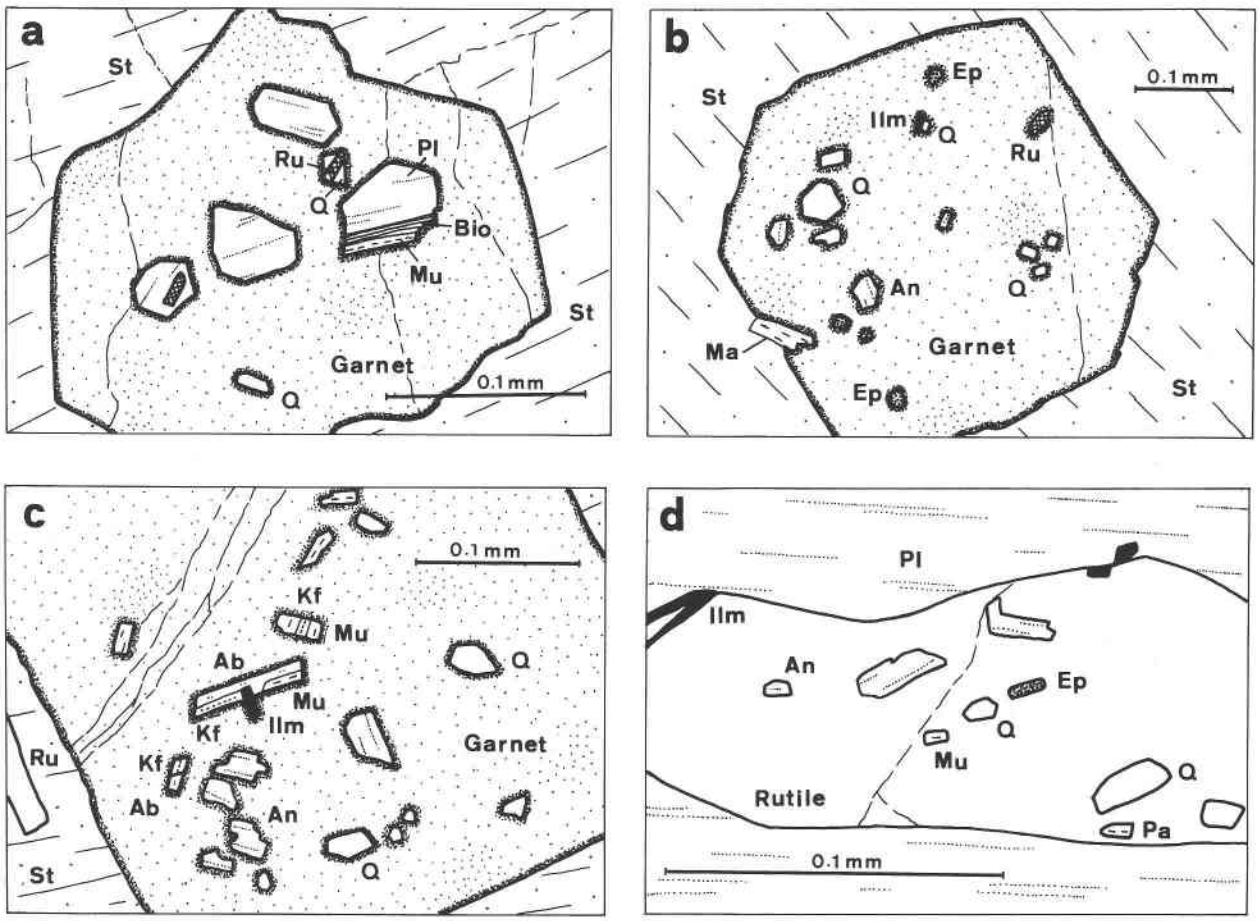

Fig. 3. Sketches from SEM photographs of microinclusions in garnet and rutile (see Table 1 for notation): (**a**) cloudy garnet (core $Gr_9Py_{10}Al_{74}Sp_7$, rim $Gr_6Py_8Al_{74}Sp_{11}$) with inclusions of plagioclase (An_{42}–An_{49}), muscovite ($Mu_{83,4,7}$), biotite ($Bio_{57,28,13}$), quartz, and rutile: (**b**) clear garnet (core $Gr_{27}Py_6Al_{62}Sp_5$, rim $Gr_{16}Py_{10}Al_{66}Sp_8$) with inclusions of anorthite (An_{91}–An_{97}), epidote (Ep_{40}), margarite (Ma_{86}), quartz, ilmenite, rutile, and pyrite; (**c**) clear garnet (core $Al_{62}Gr_{28}Py_7Sp_3$, rim $Al_{68}Gr_{13}Py_9Sp_{10}$) with inclusions of anorthite (An_{91}), albite ($Ab_{93}Kf_3$), potassium feldspar ($Kf_{94}Ab_5$), muscovite ($Mu_{100,1,7}$), quartz, and ilmenite; and (**d**) rutile with inclusions of anorthite (An_{97}), epidote (Ep_{35}), muscovite ($Mu_{85,13,6}$), paragonite ($Pa_{85}Mu_{10}$), quartz, and ilmenite.

$$= Fe_5Al_2Si_3O_{10}(OH)_8 \text{ (daphnite)} + xMgFe_{-1} + yAl_2M_{-1}Si_{-1}$$

$$Mu_{x,y,z} = K_xNa_{1-x}Mg_yFe_zAl_{3-2(y+z)}Si_{3+y+z}O_{10}(OH)_2$$

$$= NaAl_3Si_3O_{10}(OH)_2 \text{ (paragonite)} + xKNa_{-1} + yMgSiAl_{-2} + zFeSiAl_{-2}$$

where M represents the divalent octahedral cations (Fe,Mg), Al_2M_{-3} is a dioctahedral-trioctahedral mica exchange vector, and $Al_2M_{-1}Si_{-1}$ is an Mg-Fe Tschermaks exchange vector.

The composition of mineral solutions with only a single independent mixing site are specified here in the conventional way by abbreviations for the independently variable end-member components followed by subscripts indicating the mole fraction (%) of the components. The identities of these components can be deduced from Table 1. For example, the notations St_x and Ct_x indicate

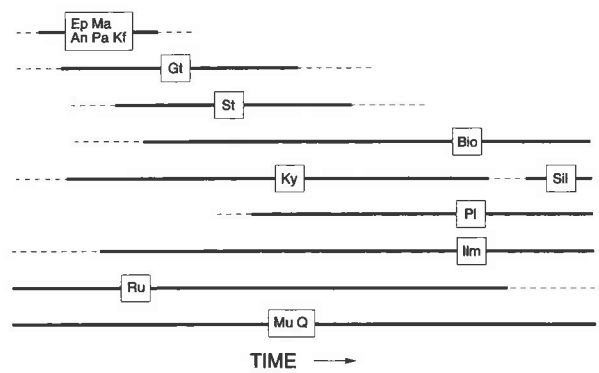

Fig. 4. Paragenetic sequence of the metapelite minerals as deduced from textural relationships. Coeval minerals, in particular microinclusions, were not necessarily in mutual equilibrium.

TABLE 1. Phase notation

Phase	Notation	Formula
Ab_xKf_y	albite	$Na_xK_yCa_{1-x-y}Al_{2-x-y}Si_{2+x+y}O_8$
$Al_xGr_yPy_z$ or Gt	garnet	$Fe_{3x}Ca_{3y}Mg_{3z}Mn_{3(1-x-y-z)}Al_2Si_3O_{12}$
An_x	anorthitic plagioclase ($x > 68$)	$Ca_xNa_{1-x}Al_{1+x}Si_{3-x}O_8$
an	stoichiometric anorthite	$CaAl_2Si_2O_8$
$Bio_{x,y,z}$	biotite	$KMg_{[3-y-3z(x)]x}Fe_{[3-y-3z(1-x)]x}Al_{1+2y+2z}Si_{3-y}O_{10}(OH)_2$
$Chl_{x,y}$	chlorite	$Mg_{[5-y]x}Fe_{[5-y](1-x)}Al_{4+2y}Si_{3-y}O_{10}(OH)_8$
Ct_x	chloritoid	$Mg_xFe_{1-x}Al_2SiO_5(OH)_2$
Do_x	dolomite	$CaMg_xFe_{1-x}(CO_3)_2$
Ep_x	epidote	$Ca_2Al_{3-x}Fe_xSi_3O_{12}(OH)$
Ilm_x	ilmenite	$Fe_{2-x}Ti_xO_3$
Kf_xAb_y	potassium feldspar	$K_xNa_yCa_{1-x-y}Al_{2-x-y}Si_{2+x+y}O_8$
Ma_x	margarite	$Ca_xNa_{1-x}Al_{3+x}Si_{3-x}O_{10}(OH)_2$
ma	stoichiometric margarite	$CaAl_4Si_2O_{10}(OH)_2$
$Mu_{x,y,z}$	muscovite	$K_xNa_{1-x}Mg_yFe_zAl_{3-2(y+z)}Si_{3+y+z}O_{10}(OH)_2$
Pa_xMu_y	paragonite	$Na_xK_yCa_{1-x-y}Al_{4-x-y}Si_{2+x+y}O_{10}(OH)_2$
Pl_x	albitic plagioclase ($x < 68$)	$Ca_xNa_{1-x}Al_{1+x}Si_{3-x}O_8$
St_x	staurolite	$Mg_{4x}Fe_{4-4x}Al_{18}Si_{7.5}O_{48}H_4$

Note: in mineral notations, *x*, *y*, and *z* represent proportions in molar percent, whereas in formulas, *x*, *y*, and *z* are absolute atomic proportions.

staurolite and chloritoid solutions containing x mol% of the Mg end-member component, respectively. If a solution involves fewer components than indicated in Table 1, then the last component is eliminated from the compositional notation. For example, the notations Kf_xAb_y and Ma_xPa_y imply potassium–sodium–calcium–alkali feldspar solution and calcium-sodium-potassium margarite solution, whereas the notations Kf_x and Ma_x imply potassium–sodium–alkali feldspar solution and calcium-sodium margarite solution.

The solution model employed for plagioclase (Newton et al., 1980) predicts a solvus with a critical composition of $X_{an} \approx 32$ mol% at $T < 667$ °C. Hence in calculated phase diagrams, at $T < 667$ °C, calcic and sodic plagioclase are distinct phases and are distinguished by the notations Pl and An, respectively.

MINERAL COMPOSITIONS

Representative mineral compositions are presented in Table 2. To permit comparison with calculated mineral compositions discussed later, the mineral compositions were normalized to the idealized forms given in Table 1. In the case of biotite, the Fe, Mg, Al, and Si contents were normalized to the formula unit $^{[6]}(Mg,Fe,Al,\square)_3{}^{[4]}(Si,Al)_4O_{10.5}$, representing the octahedral and tetrahedral site populations without consideration of the interlayer cations. Given the Fe^{3+} contents characteristic of biotite in graphitic metapelites (Guidotti and Dyar, 1991), Fe^{3+} is unlikely to have a major effect on the compositions and the inferred site occupancies.

With the exception of garnet and the microinclusions, the mineral constituents show only minor zoning and compositional variation attributable to petrographic association. Quartz, kyanite, and rutile are essentially stoichiometric. Both staurolite and biotite are nearly simple K_2O-FeO-MgO-Al_2O_3-SiO_2-H_2O (AFM) minerals. Staurolite contains a maximum of 0.2 atoms per formula unit (apfu) of non-AFM components (Ti + Mn + Zn), and its normalized composition ranges from St_{12} to St_{17} (eight analyses). Typically, biotite contains <0.1 apfu Ti and Na and has compositions in the range $Bio_{54,16,14}$–$Bio_{46,27,22}$ (eight analyses), with no evident correlation between Fe/Mg and Tschermaks substitution. Biotite that appears to replace garnet in combination with plagioclase is slightly more magnesian, with compositions between $Bio_{58,22,13}$ and $Bio_{54,30,17}$ (five analyses).

Garnets that occur within the matrix and as cloudy inclusions are similar in composition, with a slight compositional zoning manifested by an increase in spessartine component from core to rim, with a concomitant decrease in the other garnet components. The average core and rim compositions of these garnets (12 grains) are $Gr_6Py_{11}Al_{76}Sp_7$ and $Gr_6Py_{10}Al_{75}Sp_9$, respectively; the composition of the most strongly zoned garnet observed varies from $Gr_8Py_{12}Al_{73}Sp_8$ to $Gr_5Py_{10}Al_{71}Sp_{13}$. The clear garnet inclusions within staurolite are distinctly more calcic and strongly zoned, with average core and rim compositions of $Gr_{28}Py_7Al_{62}Sp_3$ and $Gr_{17}Py_{10}Al_{67}Sp_6$. In terms of grossular content, the observed extreme compositions of clear garnet are $Gr_{29}Py_6Al_{64}Sp_1$ and $Gr_{13}Py_{11}Al_{71}Sp_5$ (seven garnet grains). Thus, the clear garnets appear to represent a chemically and petrographically distinct population.

Plagioclase that occurs as inclusions within rutile and clear garnet is extremely calcic, ranging from An_{99} to An_{67}, with an average composition of An_{89} (38 analyses). In contrast, plagioclase included within cloudy garnet has a compositional range of An_{22}–An_{50} (39 analyses), with an average composition (An_{26}) similar to that of matrix (An_{23}) and porphyroblastic (An_{24}) plagioclase. For clarity in the ensuing discussion, the anorthite-rich plagioclase within clear garnet is referred to as anorthite, to distinguish it from the more sodic plagioclase that occurs elsewhere. Inclusions of muscovite also show considerable compositional variation with petrographic association. Muscovite that occurs with calc-silicate microinclusions in garnet is Na-poor ($Mu_{100,1,6}$–$Mu_{100,1,8}$, four analyses) in comparison to other muscovite that has compositions in the range $Mu_{74,4,9}$–$Mu_{86,6,6}$. Margarite (Ma_{83}–Ma_{86}, three

analyses), epidote (Ep_{34}–Ep_{40}, ten analyses), and paragonite ($Pa_{82}Mu_{11}$–$Pa_{85}Mu_{10}$, six analyses) microinclusions occur exclusively in clear garnet or rutile within porphyroblasts and show no significant compositional variations. The partitioning of Na between margarite and anorthite is identical to that reported by Bucher-Nurminen et al. (1983) for graphitic quartz + kyanite-bearing marls. This suggests that the calc-silicate microinclusions were in mutual equilibrium. Analyses of ilmenite yield ideal totals and cation stoichiometries if all Fe is considered to be Fe^{2+}. The ilmenite is homogeneous and contains no impurities other than 0.06–0.07 apfu Mn. This observation is consistent with the behavior of ilmenite predicted for quartz-bearing graphitic rocks (Connolly and Cesare, 1993).

Petrogenetic relations

The inclusion assemblages can be represented to a good approximation in the system CaO-Na_2O-MgO-FeO-Al_2O_3-SiO_2-TiO_2-C-O-H. K_2O is excluded from the analysis at this point because its presence, as manifested by inclusions of muscovite or potassium feldspar and by matrix biotite, has no influence on the calc-silicate phase relations. The chemical potentials of SiO_2, Al_2O_3, TiO_2, and C are defined by the presence of four phases of effectively fixed composition, i.e., quartz, aluminosilicate, rutile, and graphite. If the existence of a graphite-saturated C-O-H fluid phase is postulated, as suggested by the presence of fluid inclusions and graphite, then the chemical potentials of O_2 and H_2 can be expressed as a function of the fluid compositional variable X_O (Labotka, 1991; Connolly and Cesare, 1993; Connolly, 1994), where $X_O = n_O/(n_H + n_O)$. In the limit that a C-O-H fluid can be approximated as a binary CO_2-H_2O mixture, the binary compositional variable X_{CO_2} can be expressed as $X_{CO_2} \approx (3X_O - 1)/(X_O + 1)$. At any PTX_O condition, it is thus possible to determine the stable rutile-saturated ilmenite composition by minimizing μ_{FeO} as a function of composition. This value for μ_{FeO} can then be used to determine the identity and composition of the stable Mg-Fe-Al silicate (hereafter referred to as the AFM phase) and therefore the value of μ_{MgO} (this procedure is done by computer as described by Connolly, 1990). Consequently the thermodynamic degrees of freedom for the inclusion parageneses may be expressed by four variables, P, T, X_O, and X_{Ca}, where X_{Ca} is the mole fraction of Ca relative to Na. It should perhaps be emphasized that this approach is independent of any physicochemical model for the metamorphic system, i.e., closed or open system behavior, and depends only upon the validity of the inferred saturation constraints.

P-T conditions

With the above constraints, the fluid-saturated inclusion assemblage garnet + epidote + margarite + anorthite constitute a univariant equilibrium in the PTX_OX_{Ca} parametric space. Thermodynamic calculation (see Appendix 1) of the relevant petrogenetic grid shows that this

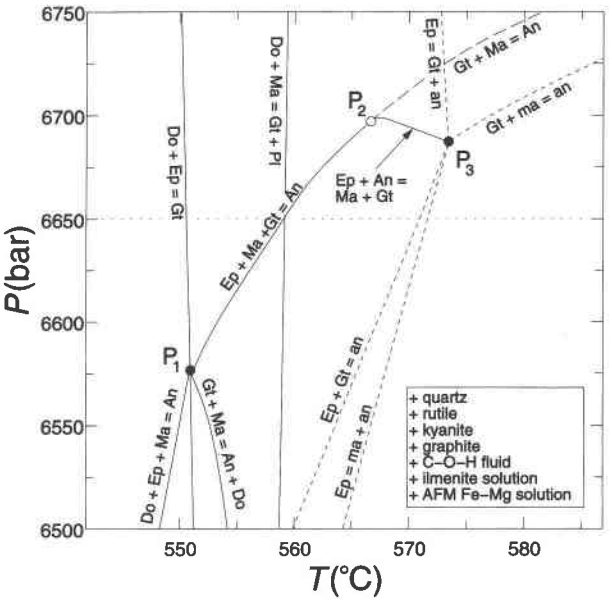

Fig. 5. Simplified P-T diagram for the system CaO-Na_2O-MgO-FeO-Al_2O_3-SiO_2-TiO_2-C-O-H after projection through quartz, kyanite, rutile, graphite, fluid, ilmenite, and the stable AFM phase, for the fluid composition range X_O = 0.333–0.667 (see Connolly and Trommsdorff, 1991, for projection methodology). Compositions of fluid, ilmenite, the AFM phase (usually chlorite), epidote, garnet, margarite, anorthite, and plagioclase vary with pressure and temperature, as determined by projection constraints. Curves labeled by corresponding reactions with high-temperature assemblages to the right of equals signs. Solid curves represent nondegenerate equilibria; dashed curves represent equilibria in a Na-free system; and the curve with long dashes corresponds to a singular equilibrium. Mineral compositions at invariant (solid circles) and singular (open circle) points are given in Table 3; notation is as in Table 1. The univariant curve An + Ep + Ma + Gt defines the possible P-T conditions for the stability of early garnet microinclusion parageneses. The univariant curve Do + Ma = Pl + Gt represents the lower thermal limit of late plagioclase + garnet assemblages. The dotted line locates isobaric T-X_O section of Fig. 7. See Appendix 1 for computational details.

equilibrium is stable only over a very restricted portion of P-T space (Fig. 5). The corresponding univariant curve extends from invariant point P_1 (Table 3), at which the assemblage becomes metastable with respect to dolomite, at 551 °C and 6584 bars, to the degenerate (Na-free system) invariant point anorthite + margarite + epidote + garnet, P_3, at 574 °C and 6685 bars (Fig. 5). At the dolomite-present invariant point, the plagioclase and margarite compositions are An_{96} and Ma_{84} and become monotonically more calcic toward the degenerate invariant point. The compositions of garnet ($Gr_{17}Py_{10}Al_{73}$) and epidote (Ep_{20}–Ep_{16}) do not change appreciably along the univariant curve. The predicted fluid composition shifts from X_O = 0.57 at P_1 toward the more H_2O-rich composition X_O = 0.42 at P_3; chlorite is the stable AFM phase at all conditions between P_1 and P_3. The calculated min-

TABLE 2. Selected mineral compositions (wt%) and cation stoichiometries

Mineral	Ab	An	Bio	Ep	Gt*	Mineral	Gt**	Ilm	Kf	Ma	Mu†
Na_2O	10.94	0.31	0.00	—	—	Na_2O	—	—	0.60	1.09	—
MgO	—	—	9.83	—	1.50	MgO	3.12	0.05	—	0.30	0.08
Al_2O_3	19.77	36.35	20.79	29.45	21.46	Al_2O_3	21.17	0.02	18.56	50.64	36.47
SiO_2	67.34	43.25	36.93	39.40	37.90	SiO_2	37.43	0.02	64.82	30.68	47.51
K_2O	0.53	—	9.19	—	—	K_2O	—	—	15.44	—	9.96
CaO	0.79	19.54	—	23.46	10.33	CaO	2.07	0.00	0.19	12.05	—
TiO_2	—	—	1.04	—	—	TiO_2	—	31.40	—	—	—
MnO	—	—	—	—	0.93	MnO	1.86	2.39	—	—	—
FeO*	—	—	18.15	6.21	28.43	FeO‡	34.78	34.42	—	0.79	1.35
H_2O	—	—	4.03	1.95	—	H_2O	—	—	—	4.47	4.56
Total	99.37	99.45	99.96	100.47	100.55	Total	100.43	99.89	99.61	100.12	99.93
Na	0.97	0.03	—	—	—	Na	—	—	0.05	0.14	—
Mg	—	—	1.09	—	0.18	Mg	0.37	0.00	—	0.03	0.01
Al	1.03	1.98	1.82	2.66	2.00	Al	2.00	0.00	1.01	3.95	2.83
Si	2.97	2.00	2.75	3.02	3.00	Si	3.00	0.00	3.00	2.03	3.13
K	0.03	—	0.87	—	—	K	—	—	0.91	—	0.85
Ca	0.04	0.97	—	1.93	0.88	Ca	0.18	0.00	0.01	0.86	—
Ti	—	—	0.06	—	—	Ti	—	1.00	—	—	—
Mn	—	—	—	—	0.06	Mn	0.12	0.07	—	—	—
Fe*	—	—	1.13	0.36	1.88	Fe‡	2.33	0.94	—	0.04	0.07
Formula	$Ab_{93}An_4$	An_{97}	$Bio_{49,24,18}$	Ep_{36}	$Al_{62}Gr_{29}Py_6Sp_2$	Formula	$Al_{77}Gr_6Py_{12}Sp_4$	Ilm_{100}	$Kf_{94}Ab_5$	Ma_{86}	$Mu_{100,1,8}$

Note: see Table 1 for notation for cation stoichiometries. H_2O content and cation stoichiometries were calculated to fit the anion stoichiometries in Table 1.

* Clear garnet, core.

** Cloudy garnet, core.

† In clear garnet.

‡ Fe^{3+} was assumed in epidote and rutile.

§ In cloudy garnet.

eral compositions are in remarkable agreement with those observed where margarite, epidote, and anorthite occur within a single garnet (An_{97} + Ep_{40} + Ma_{86} + $Gr_{27}Py_6Al_{62}Sp_5$: Fig. 3b), suggesting that the analysis is consistent and that the temperature and pressure of formation for the inclusions were in the vicinity of 550–575 °C and 6585–6685 bars.

Two points should be borne in mind when considering the phase diagrams projections shown here: (1) if a univariant equilibrium involves solution phases, then the stoichiometry of the corresponding reaction will vary continuously as a function of the variables of the diagram and (2) only phases that project into the composition space defined by the unconstrained components (i.e., thermodynamic components: Connolly, 1990) are necessary, and they are used here to define the univariant reaction. Thus, the univariant reaction Ep + Ma + Gt = An in Figure 5 can be expanded to balance the masses of all the components considered if, and only if, a P-T condition is specified, e.g., at 557 °C and 6650 bars, the anorthite-forming reaction can be expanded to 1.41 Ep_{20} + 3.26 Ma_{10} + 9.35 $Gr_{17}Py_{10}Al_{73}$ + 18.6 rutile + 0.08 fluid (X_O = 0.53) = 10.9 An_{97} + 18.8 Ilm_{99} + 1.0 $Chl_{61,60}$ + 8.91 quartz + 5.59 kyanite + 0.01 graphite. The stoichiometries of phases determined by saturation constraints (i.e., fluid, graphite, kyanite, quartz, rutile, and chlorite) should not be assigned particular importance because they could be affected by the participation of plengitic or sodic muscovite in the overall chemical reaction. In contrast, the proportions of the phases that project into the thermodynamic composition space (i.e., garnet, epidote, margarite, and anorthite or plagioclase) would not be affected by the participation of muscovite in the reaction. Accordingly, the implication that the anorthite-forming reaction, as written above, consumes a small amount of fluid with increasing temperature, although possible, must not necessarily be true for the natural process. To avoid such ambiguities, univariant equilibria are labeled here by those phases that lie within the thermodynamic composition space after projection through the compositions of the constrained components. Another possible point of confusion is that commonly the high- or low-temperature stability of an assemblage is limited by more than one equilibrium. For example, in Figure 5 (with the abbreviations given in Table 1) the low-temperature stability of anorthite is defined by the equilibria Ep + Gt = an and Ep + Ma + Gt = An; the distinction between these equilibria is that the former would only occur in the Na-free subsystem, whereas the latter would only occur in Na-bearing systems. Depending on the X_{Ca} of the system in question, the actual limit of anorthite stability may lie anywhere between these two curves.

The predicted range of PTX_O conditions for the An + Ma + Ep + Gt paragenesis should not be confused with an estimate for the uncertainty for these conditions. Such an uncertainty can be thought of as being composed of two major components representing intra- and interequilibrium factors. The intraequilibrium factor can in turn be resolved into uncertainty associated with the thermodynamic data for end-member phase components and that associated with solution models. The former uncertainty can be estimated from the variance-covariance

TABLE 2.—*Continued*

Mineral	Mu§	Pa	Pl§	Ru	St
Na_2O	1.23	6.34	8.75	—	—
MgO	0.46	—	—	0.00	1.06
Al_2O_3	37.10	40.57	23.54	0.02	53.93
SiO_2	45.89	45.85	61.07	0.02	28.48
K_2O	8.98	1.41	—	—	—
CaO	—	1.11	5.28	0.00	—
TiO_2	0.59	—	—	59.49	0.39
MnO	—	—	—	0.00	0.34
FeO‡	1.32	0.41	—	0.27	13.80
H_2O	4.55	4.69	—	—	2.17
Total	100.12	100.38	98.64	99.71	100.17
Na	0.16	0.78	0.25	—	—
Mg	0.04	—	—	0.00	0.44
Al	2.88	3.06	1.25	0.00	17.58
Si	2.92	2.93	2.75	0.00	7.88
K	0.76	0.11	—	—	—
Ca	—	0.08	0.76	0.00	—
Ti	0.03	—	—	1.00	0.08
Mn	—	—	—	0.00	0.08
Fe‡	0.07	0.02	—	0.00	3.19
Formula	$Mu_{83,4,7}$	$Pa_{81}Mu_{11}$	An_{25}	—	St_{12}

TABLE 3. Predicted mineral assemblages at selected invariant and singular points in Figs. 5–10

Point	Assemblage
P_1	$An_{96} + Ma_{84} + Al_{73}Gr_{17}Py_{10} + Ep_{20} + Do_{62} + Chl_{61,40} + Ilm_{99} + Mu_{100,4,6}$ ($X_O = 0.57$)
P_2	$An_{97} + Ma_{95} + Al_{73}Gr_{17}Py_{10} + Ep_{16} + Chl_{55,40} + Ilm_{99.2} + Mu_{100,2,8}$ ($X_O = 0.46$)
P_3	$An_{100} + Ma_{100} + Al_{73}Gr_{17}Py_{10} + Ep_{16} + Chl_{55,40} + Ilm_{99.2} + Mu_{100,2,8}$ ($X_O = 0.42$)
P_4	$Ma_{100} + Ep_{24} + Do_{33} + Ctd_8 + Ilm_{99} + Mu_{100,0,8}$
P_5	$Ma_{84} + Al_{73}Gr_{17}Py_{10} + Ep_{20} + Do_{62} + Chl_{61,40} + Ilm_{99} + Mu_{100,4,6}$
P_6	$Ma_{42} + Al_{72}Gr_{10}Py_{18} + Do_{72} + Bio_{70,20} + Ilm_{99} + Mu_{100,4,6}$
P_7	$An_{97} + Ma_{90} + Al_{73}Gr_{17}Py_{10} + Ep_{20} + Chl_{61,40} + Ilm_{99} + Mu_{100,4,6}$
P_8	$An_{100} + Ma_{100} + Ep_{16} + Chl_{55,40} + Ilm_{99.2} + Mu_{100,2,8}$
P_9	$An_{91} + Ma_{71} + Al_{75}Gr_{12}Py_{13} + Chl_{61,40} + Ilm_{99.2} + Mu_{100,4,8}$
P_{10}	$An_{44} + Ma_{48} + Al_{72}Gr_8Py_{20} + Bio_{70,30} + Ilm_{99.4} + Mu_{100,4,8}$
P_{11}	$St_7 + Chl_{44,40} + Ctd_{16} + Ilm_{99.2} + Mu_{100,2,7}$
P_{12}	$St_7 + Chl_{50,40} + Ctd_{16} + Ilm_{99.4} + Mu_{100,2,8}$
P_{13}	$Bio_{70,20} + Chl_{66,40} + Ilm_{98.8} + Mu_{100,4,8}$
P_{14}	$St_{15} + Bio_{70,20} + Chl_{61,40} + Ilm_{99.4} + Mu_{100,4,8}$
P_{15}	$St_{13} + Bio_{70,20} + Ilm_{99.4} + Mu_{100,6,8}$

Note: notation is as in Table 1. All assemblages coexist with kyanite, quartz, and rutile.

matrix provided by Holland and Powell (1990) and leads to highly correlated standard errors of $\hat{s}_P = \pm 300$ bars, $\hat{s}_T = \pm 10$ °C, and $\hat{s}_{X_O} = \pm 0.03$. Uncertainty associated with solution models is greatest for solutions that are far from end-member compositions, in this case chlorite and garnet. Error in the ideal chlorite model is unlikely to be significant in comparison with the uncertainty in chlorite end-member properties (Holland and Powell, 1990), but its quantitative assessment is too complicated to be justified here. Berman (1990) provides no error estimates for his garnet solution model, but a rough idea of this error can be deduced by comparison with the anorthite + margarite + epidote + garnet phase field computed using a garnet model derived by J. Ganguly (1993 personal communication). Discrepancies revealed by this comparison are on the order of 100 bars, 2 °C, and 0.02 mol O in the PTX_O conditions and <1 mol% in any mineral composition. Interequilibria uncertainties arise because the stability of a given phase field is determined by the stabilities of the other phases possible in the system; for example, an increase in the stability of dolomite would decrease the stability of the inclusion paragenesis as predicted in Figure 5. The computational cost of estimating this error is prohibitive, but, because of strong covariances among end-member thermodynamic data, it is unlikely to be large in comparison to intraequilibrium error.

Garnet thermobarometry and *P-T* evolution

Garnet containing anorthite inclusions occurs within the cores of staurolite porphyroblasts, whereas garnet at the rims of the staurolite porphyroblasts and within plagioclase porphyroblasts contains relatively sodic (oligoclases–andesine) plagioclase inclusions. This implies that the more calcic garnet inclusions formed earlier. As the absolute thermal limit for sodic plagioclase + garnet assemblages is defined by the Do + Ma = Gt + Pl equilibrium (Fig. 5), it can be inferred that the textural relationships record a prograde evolution with either compression or decompression. The growth of ilmenite at the expense of rutile, as occurred within the porphyroblasts, in response to Mg enrichment of staurolite, in the presence of kyanite and rutile, is also predicted to occur with increasing temperature.

The phase diagram method discussed above illustrates an approach by which physicochemical conditions are estimated from the predicted stability field for a paragenesis without explicit consideration of observed mineral compositions. An alternative approach is to attempt to match observed and predicted mineral compositions explicitly as a function of pressure and temperature. This is impractical for the full inclusion assemblages because of the number of solutions involved, but it is feasible in the subsystem CaO-MgO-FeO-Al_2O_3-SiO_2-TiO_2, an adequate model for the garnet + plagioclase + ilmenite + kyanite + quartz inclusion assemblages. Figure 6 shows the calculated stability fields for this assemblage for compositions characteristic of the early and late inclusion parageneses. In essence, this calculation amounts to the combined application of the GRAIL (Bohlen et al., 1983) and GASP (Ghent, 1976) garnet barometers, with a test for the stability of the garnet compositions within the CaO-MgO-FeO-Al_2O_3-SiO_2-TiO_2 system (Connolly, 1990). As might be anticipated, since both the GRAIL and GASP mineral component equilibria are commonly used as barometers, there is a large uncertainty associated with the estimated temperatures. This uncertainty is compounded by the effect of spessartine solution, particularly in the late garnets, which would tend to lower the predicted pressures. Despite this, both early and late garnet + plagioclase compositions are consistent with a relatively flat *P-T* trajectory of 150 °C/kbar, beginning at a low temperature and passing through the conditions inferred for the full inclusion paragenesis. This suggests that

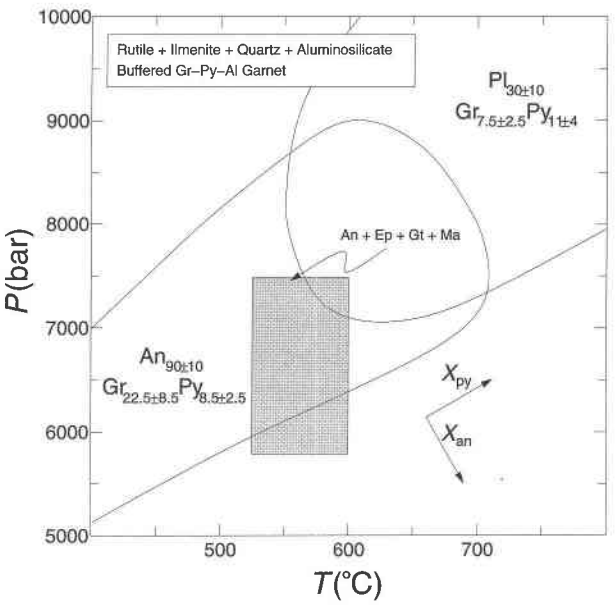

Fig. 6. Predicted P-T stability fields for observed garnet and plagioclase compositions in the rutile + ilmenite + aluminosilicate + quartz–saturated system CaO-Na_2O-MgO-FeO-Al_2O_3-SiO_2-TiO_2. Stability fields include a 95% ($\delta_P \approx \pm$ 380 bars: Kohn and Spear, 1991) confidence interval for pressure. The shaded rectangle locates the 95% confidence interval for conditions for An + Ep + Gt + Ma paragenesis (Fig. 5). The arrows in the lower right corner indicate approximate directions in which anorthite content in plagioclase and pyrope content in garnet increase with pressure and temperature. See Appendix 1 for computational details.

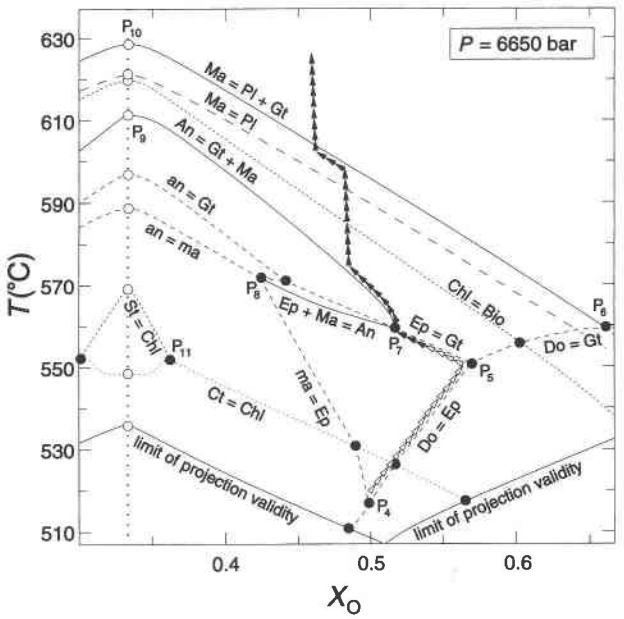

Fig. 7. Isobaric (P = 6650 bars) T-X_O phase diagram section for the system shown in Fig. 5, with the additional constraint that all phase relations are stable with phengitic muscovite. Curves are labeled by reactions with high-temperature assemblages to the right of equals signs. Maximum H_2O activity occurs at X_O = ⅓ (vertical dotted line) in C-O-H fluids (Connolly and Cesare, 1993). Solid curves represent nondegenerate equilibria; dashed curves represent Na-free equilibria; short-dashed curves represent AFM phase relations. Solid arrows indicate T-X_O evolution of inclusions and matrix calc-silicates, as inferred from textural relationships. Open arrows illustrate a T-X_O path given that the high-X_O fluid composition originated from the decarbonation of dolomite. Mineral compositions at selected invariant (solid circles) and singular (open circles) points are given in Table 3; notation is as in Table 1. See Appendix 1 for computational details.

at least the early garnet inclusions formed prior to the major phase of regional decompression documented by Franceschelli et al. (1989).

The accuracy of the requisite thermodynamic models and the possibility of compositional reequilibration do not warrant further speculation on the nature of the metamorphic P-T relationship, and, for purposes of understanding petrogenetic relationships, the metamorphism will be considered to have been isobaric (P = 6650 bars). This simplification may affect the quantitative results but not the qualitative behavior of the system.

Fluid evolution

Given the assumption of isobaric metamorphism, the role of fluid composition during the evolution of the inclusions can be shown by constructing a T-X_O section through the P-T diagram of Figure 5, as shown in Figure 7. Biotite becomes the stable AFM phase that coexists with ilmenite + quartz + rutile + kyanite + graphite + fluid at high temperature, and, to permit calculation of phase relations at such conditions, saturation with respect to phengitic (Na-free) muscovite was assumed. Figure 8 illustrates the compositional phase relations in Figure 7 as a function of temperature and X_{Ca} at an arbitrary fluid composition (X_O = 0.45); the peritectoids and eutectoids of Figure 8 correspond to the univariant curves of Figure 7. For simplicity, K components were not considered in the margarite and plagioclase models; therefore, the phase relations at Na-rich compositions ($X_{Ca} < 0.1$) in Figure 8 are not reliable. For this reason, only phase equilibria that occur in systems more calcic than the Ma = Pl singular point (X_{Ca} = 0.14: Fig. 8) are shown in the T-X_O projection (Fig. 7). In the T-X_O projection, the univariant curve An + Ma + Ep + Gt of Figure 5 appears as the isobaric invariant point P_7. If fluid composition is externally controlled, the probability of such an equilibrium is zero; thus the occurrence of the invariant point assemblage implies that fluid composition was buffered by the degenerate (margarite-present) univariant T-X_O garnet + epidote equilibrium. At the invariant point, anorthite and garnet would form at the expense of margarite and epidote until epidote was consumed or isolated within garnet. With additional heating, the system would be buffered along the An = Ma + Gt univariant curve. Once anorthite reacted out, the fluid composition would be buffered to lower X_O by isobarically divariant margarite de-

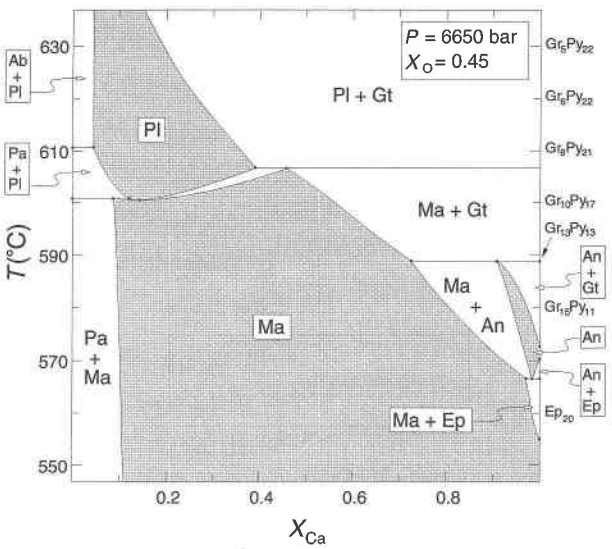

Fig. 8. Isobaric (P = 6650 bars), constant-X_O, T-X_{Ca} phase diagram illustrating phase relations from Fig. 7 at X_O = 0.45. Notation is as in Table 1; see Appendix 1 for computational details.

hydration (if one ignores the possible effects of AFM reactions discussed below). The T-X_O path during divariant dehydration cannot be constrained without knowledge of the bulk composition of the system, but the divariant buffering effect would be small in any case and is neglected in the path shown in Figure 7. Significant buffering would resume with the isobarically univariant formation of relatively sodic plagioclase, as observed in the late-stage cloudy garnets, by the reaction of margarite and garnet. The latter part of this sequence of mineral reactions is identical to that obtained for Ca-rich compositions in Figure 8, with increasing temperature, and the range of predicted mineral compositions (constrained by the invariant and singular points of Figs. 7 and 8 and Table 3) compare well with those observed (Table 4).

Fluid produced by simple dehydration is constrained to have the composition X_O = ⅓; thus the inferred fluid compositions require a significant enrichment in O component, most plausibly from CO_2. It is unlikely that this component was derived by fluid infiltration because infiltration would overwhelm the buffering capacity of the calc-silicate mineral assemblage. Therefore the decomposition of a carbonate is the most probable source of a high-X_O fluid. As can be seen in Figure 7, dolomite is a reasonable candidate for this carbonate in terms of phase equilibria. The low-temperature portion of the path in Figure 7 illustrates a hypothetical T-X_O evolution, with the assumption that dolomite was stable at low temperature. The presence of dolomitic segregations within the pelite protolith would explain the unusually calcic composition of the microinclusions. Direct macroscopic and other microscopic evidence for such segregations is lacking in the metapelite sample, but calc-silicate segregations occur within a few meters of the sample locality (Elter et al., 1986).

Table 4. Summary of observed and calculated mineral compositions

Mineral	Observed composition	Predicted composition
Albite	$Ab_{93}Kf_1$	Ab_{95}
Anorthite	An_{67}–An_{99}	An_{91}–An_{100}
Biotite	$Bio_{46,27,22}$–$Bio_{58,22,13}$	$Bi_{70,20}$–$Bi_{70,30}$
Epidote	Ep_{34}–Ep_{40}	Ep_{16}–Ep_{24}
Early garnet	$Gr_{13}Py_{11}Al_{71}Sp_5$–$Gr_{29}Py_6Al_{60}Sp_5$	$Gr_{12}Py_{13}Al_{75}$–$Gr_{17}Py_{10}Al_{73}$
Late garnet	$Gr_5Py_{10}Sp_{13}Al_{71}$–$Gr_8Py_{12}Sp_8Al_{72}$	$Gr_5Py_{22}Al_{73}$–$Gr_8Py_{21}Al_{71}$
Ilmenite	Ilm_{100}	$Ilm_{98.8}$–$Ilm_{99.4}$
Potassium feldspar	$Kf_{94}Ab_5$	Kf_{67}–Kf_{80}
Early margarite	Ma_{83}–Ma_{86}	Ma_{71}–Ma_{100}
Muscovite	$Mu_{74,4,9}$–$Mu_{100,1,8}$	$Mu_{83,4,8}$–$Mu_{100,2,8}$
Paragonite	$Pa_{82}Mu_{11}$–$Pa_{85}Mu_{10}$	Pa_{81}–Pa_{100}
Plagioclase	An_{23}–An_{50}	An_{12}–An_{44}
Staurolite	St_{12}–St_{17}	St_7–St_{15}

The existence of a high-X_O fluid also provides an explanation for the occasional presence of potassium feldspar and albite rather than muscovite or paragonite in the early garnet inclusions. If the quartz + kyanite saturated system K_2O-Na_2O-Al_2O_3-SiO_2-C-O-H is taken as a model for these inclusions, the assemblage potassium feldspar ($Kf_{94}Ab_5$) + albite ($Ab_{93}Kf_3$) + anorthite (An_{91}) + muscovite ($Mu_{100,1,7}$) + quartz (Fig. 3c) represents conditions at the onset of the muscovite breakdown reaction. At the P-T conditions inferred for the garnet + epidote + margarite + anorthite inclusion assemblage (ca. 550 °C, 6650 bars), this implies a fluid composition of $X_O \approx$ 0.85 (Fig. 9). The extent of solid solution in the minerals is somewhat more limited than predicted (Fig. 9), and whereas this may reflect reequilibration, it may also indicate a lower temperature of formation and therefore even more O-rich fluid composition. The compositional width of the plagioclase solvus represented by the inclusion assemblage also suggests lower temperatures. It is noteworthy that the inclusion assemblage would have been metastable with respect to granitic melt had it formed in the presence of more H_2O-rich fluids. The absence of any evidence for partial melting thus also supports the presence of high-X_O fluid.

AFM minerals

The sequence of calc-silicate reactions discussed in the previous section is capable of controlling fluid composition, provided no other major reactions involving the fluid components took place contemporaneously. In this respect, the most probable reactions of this type are those involving AFM minerals. Ignoring the effect of minor solution behavior, at an arbitrary PTX_O condition only one AFM mineral may be stable in addition to the assemblage quartz + rutile + ilmenite + kyanite + muscovite. The calculated T-X_O stability fields for the AFM minerals at 6650 bars are shown in Figure 7 by dashed curves, where it can be seen that the predicted and observed AFM mineral assemblages are not consistent because the stability field of chlorite separates those of staurolite and

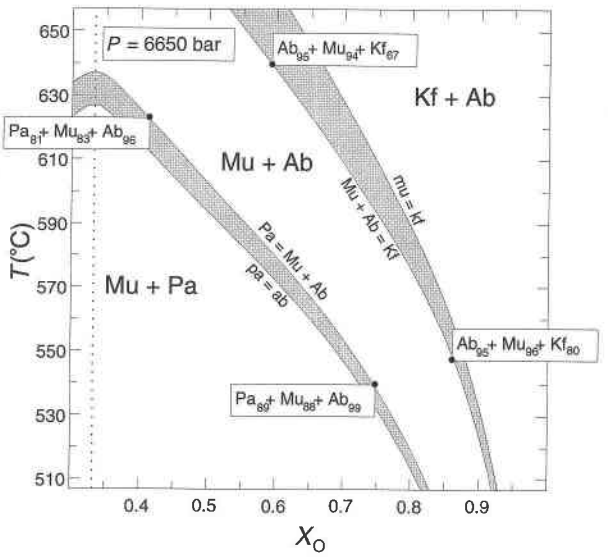

Fig. 9. Isobaric (P = 6650 bars) T-X_O phase diagram section for the quartz + kyanite + graphite–saturated system Na_2O-K_2O-Al_2O_3-SiO_2-C-O-H. Substantially more O-rich fluid compositions than those inferred for calc-silicate microinclusons (point P_7: Fig. 8) are required to explain albite + muscovite and orthoclase + albite associations observed in early garnet. The vertical dotted line locates the X_O = ⅓ fluid composition. Mineral compositions at selected invariant (solid circles) points are given in Table 3; notation is as in Table 1. See Appendix 1 for computational details.

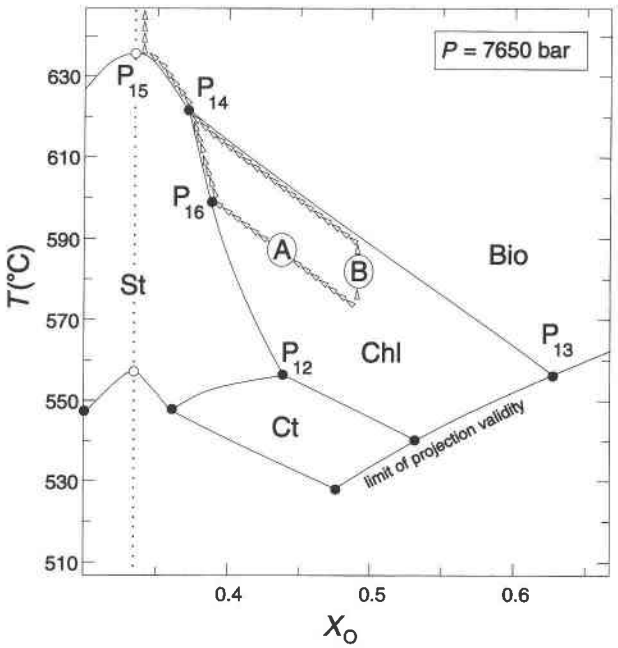

Fig. 10. Isobaric (P = 7650 bars) T-X_O phase diagram section showing stable AFM phases in the rutile + quartz + kyanite + graphite + ilmenite–saturated system MgO-FeO-K_2O-Al_2O_3-SiO_2-TiO_2-C-O-H. The vertical dotted line locates the X_O = ⅓ fluid composition. Arrows indicate possible T-X_O evolution paths for the fluid phase.

biotite. Aside from questioning the validity of the computational assumptions and thermodynamic data, a simple explanation for this inconsistency is that Fe^{3+} and Ti solution as well as dioctahedral-trioctahedral mica exchange (which are not considered in the AFM mineral models) expand the stability field of biotite relative to chlorite (see also Powell and Holland, 1990). However, the AFM mineral stability fields are also sensitive to pressure such that an increase of 1000 bars in the estimated pressure results in a T-X_O topology (Fig. 10) that is in qualitative agreement with the inferred petrogenesis. [The AFM topology can be brought into quantitative agreement with the inferred petrogenesis by decreasing the estimated Gibbs energies of staurolite by 0.6 kJ/mol and biotite by 0.9 kJ/mol. Such adjustments are within the uncertainties of Holland and Powell's (1990) estimates but may not be warranted because of the covariance of the estimates, as well as the effects of non-AFM components, as discussed above.] Given the validity of this topology, the calc-silicate microinclusions may have formed in the chlorite stability field. There are then two possible fluid evolution paths. If the An = Gt + Ma (Fig. 8) dehydration reaction buffers fluid composition over an extended range of X_O, then T-X_O conditions are driven toward the St = Chl hydration equilibrium (P_{16}, path A: Fig. 10). Staurolite then forms until margarite is exhausted; whether the St = Chl equilibrium buffers fluid composition beyond this point depends on the relative mineral proportions. Such a path has the merit that it explains the absence of sodic margarite within the garnets, as would be expected if the T-X_O evolution were unperturbed by AFM mineral reactions (as shown in Fig. 7). Alternatively, if the An = Gt + Ma equilibrium ceased buffering the fluid composition before staurolite formed, the fluid composition would be unbuffered until biotite began to form (path B: Fig. 10). The Chl = Bio dehydration reaction would then provide a strong fluid composition buffer. In either case, a major episode of H_2O-rich fluid production would occur at the staurolite + chlorite + biotite invariant point. Such an episode of voluminous fluid production accounts for the transition from conditions of grain-scale mosaic equilibrium (Korzhinskii, 1959), which prevailed during the formation of the calc-silicate inclusions, to the nearly overall equilibrium presented by the metapelite matrix. Thereafter, staurolite and biotite would coexist over a short temperature interval terminated by the thermal stability limit of staurolite. Except for the absence of sodic margarite, petrographic evidence for the alternative sequences is equivocal because the temporal relationship between biotite and staurolite is unclear. The ranges of predicted compositions for biotite and staurolite are in reasonable agreement with those observed (Table 4). In considering the T-X_O diagrams of Figures 7, 9,

and 10, it must be noted that the stability field of the chemical potential buffering assemblage graphite + rutile + ilmenite + kyanite becomes restricted to progressively more Fe-rich bulk compositions with decreasing temperature until it is terminated by conditions at which Mg-free, Fe silicates or carbonates may coexist with rutile (the limit of projection validity in Figs. 7 and 10). Thus, it is unlikely that this buffer existed at temperatures much lower than those estimated for the inclusions, and therefore the calculated phase relations cannot be used to infer the preinclusion mineralogy of the pelite.

Conclusions

Analysis of the anorthite + epidote + margarite microinclusions within garnets included in the cores of staurolite porphyroblasts indicates the presence of a relatively CO_2-rich ($X_O > 0.5$) fluid at an early stage in the prograde pelite metamorphism, a result supported by fluid inclusion evidence. The composition of this fluid was controlled by mineral reactions, which suggests that externally derived fluid did not play a major role in this stage of the metamorphism. The probable sources of this fluid were minute carbonate-rich segregations. The small quantity and low H_2O content of fluid produced by decarbonation inhibited transport processes and resulted in mosaic equilibria, as well as in the fine grain size of the inclusions. The existence of such segregations, in conjunction with a mosaic equilibrium model (Korzhinskii, 1959), explains the heterogeneity of the early inclusions and the calcic mineral compositions. Conditions of mosaic equilibrium must have prevailed prior to, or during a hiatus in, dehydration of the bulk mineralogy. The eventual dehydration of staurolite, or perhaps of chlorite, generated more voluminous quantities of H_2O-rich fluid and caused a closer approach to overall equilibrium as represented by the matrix mineralogy. This model suggests that pervasive fluid infiltration was not important and that the fluid produced by devolatilization was effectively isolated from the rock on a local scale. Similar conclusions, though for a lower grade of metamorphism, may be drawn from the study of Burton and O'Nions (1991), where phase equilibria indicated that an essentially pure CO_2 fluid was present in layers 1–2 cm thick of a graphitic pelite during the onset of metamorphism, and that this fluid did not influence mineral equilibria in adjacent layers.

Acknowledgments

The authors are indebted to J. Brady, A. Léger, V. Lopez Sanchez-Vizcaino, and an anonymous reviewer for constructive reviews. D. Sidler is thanked for the electron microprobe analyses done at the Swiss Federal Institute of Technology and for her explanation of mica normalization schemes. T. Holland kindly provided the program Thermocalc (Powell and Holland, 1990), used to estimate uncertainties associated with the thermodynamic data. Financial support from Italian Ministry of Universities and Scientific and Technological Research grants (MURST, to C.A.R. and I.M.) and Swiss National Science Foundation grants 21-36503.93 (to J.A.D.C.) and 2000-037388.93/1 (to V.T.) is gratefully acknowledged.

References cited

Anderson, D.J., and Lindsley, D.H. (1988) Internally consistent solution models for Fe-Mg-Mn-Ti oxides. American Mineralogist, 73, 714–726.

Berman, R.G. (1990) Mixing properties of Ca-Mg-Fe-Mn garnets. American Mineralogist, 75, 328–344.

Bohlen, S.R., Wall, V.J., and Boettcher, A.L. (1983) Experimental and geological implications of equilibria in the system FeO-TiO_2-Al_2O_3-H_2O. American Mineralogist, 68, 1049–1058.

Bucher-Nurminen, K., Frank, E., and Frey, M. (1983) A model for the progressive metamorphism of margarite-bearing rocks in the Central Alps. American Journal of Science, 283A, 370–395.

Burton, K.W., and O'Nions, K.K. (1991) High resolution garnet chronometry and the rates of metamorphic processes. Earth and Planetary Science Letters, 107, 649–671.

Chatterjee, N.D., and Froese, E. (1975) A thermodynamic study of the pseudobinary join muscovite-paragonite in the system $KAlSi_3O_8$-$NaAlSi_3O_8$-Al_2O_3-SiO_2-H_2O. American Mineralogist, 60, 985–993.

Connolly, J.A.D. (1990) Calculation of multivariable phase diagrams: An algorithm based on generalized thermodynamics. American Journal of Science, 290, 666–718.

——— (1994) Phase diagram methods for graphitic rocks and an application in the system C-O-H-FeO-TiO_2-SiO_2. Contributions to Mineralogy and Petrology, in press.

Connolly, J.A.D., and Cesare, B. (1993) C-O-H-S fluid composition and oxygen fugacity in graphitic metapelites. Journal of Metamorphic Geology, 11, 379–388.

Connolly, J.A.D., and Trommsdorff, V. (1991) Petrogenetic grids for metacarbonate rocks: Pressure-temperature phase-diagram projection for mixed-volatile systems. Contributions to Mineralogy and Petrology, 108, 93–105.

Elter, F.M., Franceschelli, M., Ghezzo, C., and Ricci, C.A. (1986) The geology of northern Sardinia. International Geological Conference Proceedings, 5, 87–102.

Franceschelli, M., Memmi, I., and Ricci, C.A. (1982) Ca distribution between almandine-rich garnet and plagioclase and psammitic schists from the metamorphic basement of north-eastern Sardinia. Contributions to Mineralogy and Petrology, 80, 285–295.

Franceschelli, M., Memmi, I., Pannuti, F., and Ricci, C.A. (1989) Diachronus metamorphic equilibria in the Hercynian basement of northern Sardinia, Italy. In J.S. Daly, R.A. Cliff, and B.W.D. Yardley, Eds., Evolution of metamorphic belts. Geological Society Special Publication, 43, 371–375.

Ghent, E.D. (1976) Plagioclase-garnet-Al_2SiO_5-quartz: A potential geobarometer-geothermometer. American Mineralogist, 61, 710–714.

Guidotti, C.V., and Dyar, M.D. (1991) Ferric iron in metamorphic biotite and its petrologic and crystallochemical implications. American Mineralogist, 76, 161–175.

Hillert, M. (1980) Empirical methods of predicting and representing thermodynamic properties of ternary solution phases. CALPHAD, 4, 1–12.

Holland, T.J.B., and Powell, R. (1990) An enlarged and updated internally consistent dataset with uncertainties and correlations: The system K_2O-Na_2O-CaO-MgO-Mn-FeO-Fe_2O_3-Al_2O_3-TiO_2-SiO_2-C-H_2-O_2. Journal of Metamorphic Geology, 8, 89–124.

Kohn, M.J., and Spear, F.S. (1991) Error propagation for barometers. I. Accuracy and precision of experimentally located end-member reactions. American Mineralogist, 76, 128–137.

Korzhinskii, D.S. (1959) Physiochemical basis of the analysis of the paragenesis of minerals, p. 19. Consultants Bureau, New York.

Labotka, T.C. (1991) Chemical and physical properties of fluids. Mineralogical Society of America Reviews in Mineralogy, 26, 43–104.

Newton, R.C., Charlu, T.V., and Kleppa, O.J. (1980) Thermochemistry of the high structural state plagioclases. Geochimica et Cosmochimica Acta, 44, 933–941.

Powell, R., and Holland, T.J.B. (1990) Calculated mineral equilibria in the pelite system, KFMASH (K_2O-MgO-FeO-Al_2O_3-SiO_2-H_2O). American Mineralogist, 75, 367–386.

Thompson, J.B. (1981) An introduction to the mineralogy and petrology of the biopyriboles. Mineralogical Society of America Reviews in Mineralogy, 9A, 141–186.

Thompson, J.B., and Waldbaum, D.R. (1969) Mixing properties of sanidine crystalline solutions. IV. Phase diagrams from equations of state. American Mineralogist, 54, 1274–1298.

Whitney, D.L. (1991) Calcium depletion haloes and Fe-Mn-Mg zoning around faceted plagioclase inclusions in garnet from a high grade pelitic gneiss. American Mineralogist, 76, 493–500.

Manuscript received March 25, 1993
Manuscript accepted April 15, 1994

Appendix 1. Thermodynamic models and calculations

All phase equilibrium calculations reported here were done with the mineral end-member data of Holland and Powell (1990) and the computer program described by Connolly (1990). The Fortran source code and data files for the program (Perplex) are available upon request from the senior author of this work. The program Thermocalc (Powell and Holland, 1990) was used to estimate uncertainties associated with the end-member thermodynamic data. Mixing properties of mineral solutions were taken from Anderson and Lindsley (ilmenite-hematite: 1988), Berman (grossular-almandine-pyrope: 1990), Chatterjee and Froese (for muscovite-paragonite in the calculation of Fig. 9: 1975), Newton et al. (anorthite-albite: 1980), and Thompson and Waldbaum (sanidine-albite: 1969). All other mineral solutions (epidote, margarite, staurolite, chlorite, biotite, and phengitic muscovite) were treated as ideal. For these solutions, the site occupancies suggested by Holland and Powell (1990) were assumed; for phengitic muscovite, chlorite, and biotite, these take into account Fe-Mg substitution and Tschermaks type substitutions. Properties of graphite-saturated C-O-H fluids were computed as described by Connolly and Cesare (1993).